

# Quantifying mass balance processes on the Southern Patagonia Icefield

M. Schaefer<sup>1,2</sup>, H. Machguth<sup>3</sup>, M. Falvey<sup>4</sup>, G. Casassa<sup>5,6</sup>, and E. Rignot<sup>7,8</sup>

<sup>1</sup>Instituto de Ciencias Físicas y Matemáticas, Facultad de Ciencias, Universidad Austral de Chile

<sup>2</sup>Instituto de Ciencias Marinas y Limnológicas, Facultad de Ciencias, Universidad Austral de Chile

<sup>3</sup>Arctic Technology Centre, Technical University of Denmark, Kgs. Lyngby, Denmark.

<sup>4</sup>Department of Geophysics, Universidad de Chile, Santiago, Chile.

<sup>5</sup>Geostudios, Las Vertientes, San José de Maipo, Chile.

<sup>6</sup>Universidad de Magallanes, Punta Arenas, Chile.

<sup>7</sup>Jet Propulsion Laboratory, Pasadena, USA

<sup>8</sup>University of California, Department of Earth System Science, Irvine, USA

**Abstract.** We present surface mass balance simulations of the Southern Patagonia Icefield driven by downscaled reanalysis data. The simulations were evaluated and interpreted using geodetic mass balances, measured point balances and a complete velocity field of the Icefield from spring 2004. The high measured accumulation of snow of up to 15.4 meters water equivalent per year as well as the high measured ablation of up to 11 meter water equivalent per year is reproduced by the model. The overall modeled surface mass balance was positive and increasing during 1975-2011. Subtracting the surface mass balance from geodetic balances, calving fluxes were inferred. Mass losses of the SPI due to calving were strongly increasing from 1975-2000 to 2000-2011 and higher than losses due to surface melt. Calving fluxes were inferred for the individual glacier catchments and compared to fluxes estimated from velocity data. Measurements of ice thickness and flow velocities at the glaciers' front and spatially distributed accumulation measurements can help to reduce the uncertainties of the different terms in the mass balance of the Southern Patagonia Icefield.

## 1 Introduction

The Southern Patagonia Icefield (SPI, Fig. 1) is the largest ice mass in the Southern Hemisphere outside of Antarctica. The great majority of its outlet glaciers have been retreating and thinning at high rates in recent decades (Rignot et al., 2003; Masiokas et al., 2009; López et al., 2010; Willis et al., 2012b; Davies and Glasser, 2012; White and Copland, 2013). Mass balance processes for most of the glaciers of the SPI, however, are poorly quantified, which makes it difficult to understand the reasons for the fast ice loss from the SPI. Increase in surface melt, decrease in accumulation or changes in the

ice dynamics are possible candidates. Another explanation could be sub-glacial volcanic activity (Orihashi et al., 2004) which is motivated by the fact that the SPI coincides with four volcanoes of the Andean Austral Volcanic Zone (Stern, 2004, 2008).

Locally varying warming trends have been observed in Southern South America in the last century with rates up to 0.028 °C/year next to the Atlantic Ocean (Rosenblüth et al., 1995; Ibarzabal y Donangelo et al., 1996; Rasmussen et al., 2007; Falvey and Garreaud, 2009). Large inter-annual and inter-decadal variations of precipitation have been observed in Patagonia, although with no significant overall trends in the last century (Rosenblüth et al., 1995; Carrasco et al., 2002; Aravena and Luckman, 2009).

Prominent acceleration of the ice flow ( and therefore ice loses due to calving) were detected at the Glaciers Jorge Montt (Rivera et al., 2012a) and Upsala (Jaber et al., 2012; Sakakibara et al., 2013). For both glaciers a fast retreat of the glacier was observed together with the acceleration.

The surface mass balance was modeled for two glaciers of the SPI: Chico Glacier (Rivera, 2004) and Perito Moreno Glacier (Stuefer et al., 2007), both using degree-day-models. For the period 1975-2001 Rivera (2004) obtained an average negative yearly surface mass balance of Chico Glacier, which was showing high inter-annual variations and a slightly negative trend. Stuefer et al. (2007) obtained a near to zero cumulative glacier mass balance for the Perito Moreno Glacier between 1973 and 2000, with the annual specific balances varying between +1 and -1 meter water equivalent (mweq).

A combined modeling approach was recently applied on the Northern Patagonia Icefield (NPI) (Schaefer et al., 2013): global meteorological data were downscaled using the regional climate model Weather Research and Forecasting and statistical downscaling techniques. These data were used to drive a surface mass balance model of intermediate complexity (Oerlemans, 2001; Machguth et al., 2009). An increase of accumulation was detected over the NPI during

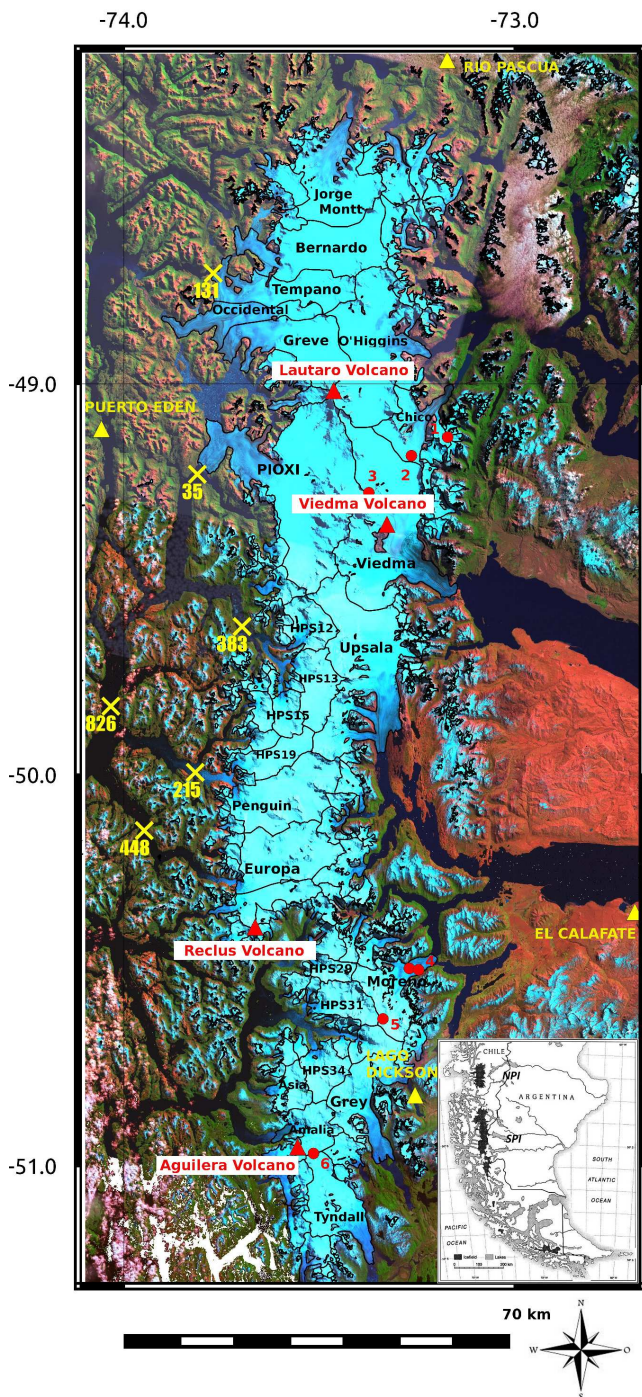


**Fig. 1.** The Southern Patagonia Icefield (SPI): false-colour composite of Landsat ETM+ satellite image mosaic; names of examined glacier catchments in black; yellow triangles mark the positions of some of the meteorological stations that were used to validate the downscaling of the reanalysis data; red dots mark direct surface mass balance measurements on the SPI (1-6); the four active volcanoes that coincide with the SPI are represented by red triangles. The yellow crosses with numbers mark individual measurements of fjord depth provided by the Chilean Navy Hydrographic and Oceanographic Service (SHOA). Inset: position of the SPI in Southern South America.

1975-2011. The increased observed mass loss of the NPI in 2000-2011 (Willis et al., 2012a) as compared to 1975-2000 (Rignot et al., 2003) was explained by an increase of losses by calving.

In this paper a similar methodology is applied to make first inferences of the components of the mass balance of the SPI as a whole and for its individual glacier catchments. We give a summary of the methods applied in Section 2. In Section 3 we present the results, discuss them and in Section 4 we draw the conclusions of our study.

## 2 Methods

To obtain realistic meteorological input data for the surface mass balance model in the modeling period 1975-2011, a downscaling procedure has been realized, which includes a number of steps (Schaefer et al., 2013). As a first step, version 3.2 of the Advanced Research Weather Research and Forecasting model (WRF-model hereafter) was run for a 7 year period from 2005 until 2011, using a nested computational grid (five point relaxation zone between grids), with the inner grid having a spatial resolution of 5 km over an area of 675 km x 425 km that includes both the NPI and SPI. The model was forced at its boundaries by NCEP-NCAR atmospheric reanalysis data (Kalnay et al., 1996), which consist of three-dimensional atmospheric fields on a 2.5° resolution grid at 6 hour intervals. The WRF-model's output was saved at hourly intervals, which were used to yield the daily averages required by the surface mass balance model. To obtain downscaled meteorological data for the entire 1975-2011-period, statistical downscaling techniques were applied similar to the ones used to relate local climate observations to large scale atmospheric parameters that are predicted by low resolution Global Circulation Models (Fowler et al., 2007). The basic assumption is that local variability (which in this case is simulated rather than observed) is to a large extent controlled by the overriding synoptic conditions, and that long-term changes in these synoptic conditions are the key drivers of long-term changes in local variables. The series of daily fields of precipitation, temperature and incoming shortwave radiation for the period 2005-2011 are modeled in terms of 11 predictors taken from the NCEP-NCAR reanalysis data at a grid point some 250 km upstream (west) of the NPI, which include atmospheric temperature, relative humidity, zonal moisture flux and meridional moisture flux at different pressure levels (Schaefer et al., 2013). The correlations between the daily averaged output of the WRF-model and the statistical downscaling technique at the different grid points range between 0.65 and 0.80 for precipitation, 0.85-0.93 for temperature and 0.56-0.77 for solar radiation and indicate that the statistical downscaling is applicable.

A further downscaling of the input data of the mass balance model is realized to obtain input data with a resolution of 180 m, the resolution used for the surface mass balance

model. Temperature and precipitation are “physically interpolated” by applying constant lapse rates ( $-0.65^{\circ}\text{C}/100\text{ m}$  and  $5\%/100\text{ m}$ , respectively) and incoming solar radiation on the 180 m grid is computed by comparing the radiation computed for the 5 km-grid with calculations from clear-sky radiation on the 180 m-grid (Schaefer et al., 2013; Corripio, 2003).

In the surface mass balance model ablation was calculated according to a simplified energy balance model (Oerlemans, 2001; Machguth et al., 2009): the net short-wave radiation was determined by the incoming solar radiation and three different albedo values for snow (0.7), firn (0.45) and ice (0.3), whilst the sum of the net long-wave radiation and the turbulent fluxes was approximated by a linear function of the air temperature. Since the SPI is situated in a relatively mild, maritime climate, the ice is supposed to be temperate, so that we assume that ice which melts at the surface will not refreeze but immediately run off from the SPI. Accumulation at every grid cell was defined as solid precipitation, which is as a fraction of the total precipitation that varied between zero and one depending on the air temperature of the grid cell (Schaefer et al., 2013).

### 3 Results and Discussion

#### 3.1 Climate

The result of the downscaling process are daily maps of the surface mass balance input variables temperature, incoming solar radiation and precipitation at the resolution of the mass balance model. In Fig. 2a, we present the annual mean incoming solar radiation (averaged over 1975-2011). The radiation pattern can be divided in two main parts: the central and western part of the icefield, where yearly average incoming solar energy is below  $70\text{ W/m}^2$ , and the eastern part which corresponds to the lower part of the eastern outlet glaciers, where the incoming solar radiation is much higher, reaching values of up to  $150\text{ W/m}^2$  on some glacier tongues. On the tongues of some north-western outlet glaciers, the incoming solar radiation is also higher than in the central part of the icefield (up to  $100\text{ W/m}^2$ ). These results of incoming solar radiation reflect well the climatic situation on the SPI, where nearly all year long clouds are blocked by the high peaks of the icefields, which reduce the incoming solar radiation. East of the high peaks cloudiness decreases and incoming solar radiation increases. Several glacier tongues in the north-west of the icefield reach out of this permanent sea of clouds and receive more solar radiation than the center part of the icefield. The downscaled average precipitation map shows a strong increase with elevation due to the generation of orographic precipitation in the regional climate model. East from the Andes main ridge the modeled precipitation decreases rapidly. The temperature decreases with elevation as expected. The results of the downscaling of the

meteorological data was compared in detail to meteorological data (Schaefer et al., 2013). Subsequently a calibration of the surface mass balance model has been realized using mass balance measurements in the NPI. Since the climatological situation on the SPI is very similar to the NPI we use the same calibration for the SPI and present surface mass balance simulations for the set of model parameters that performed best on the NPI (Schaefer et al., 2013).

#### 3.2 Distributed surface mass balance

In Fig. 2b we present the distributed annual surface mass balance averaged over 1975-2011. Very positive surface mass balance of up to 20 meter water equivalent (mweq) is obtained for the very high peaks of the icefield. On the flat plateau the surface mass balance is between 0 and 5 mweq and on the outlet glacier tongues it reaches down to  $-15\text{ mweq}$ . The direct (point) observations of the surface mass balance on the SPI are restricted to a network of ablation stakes with changing configuration on the Perito Moreno Glacier during 1995 and 2003 (Stuefer et al., 2007), a tower installed near the equilibrium line of Glacier Chico where yearly surface mass balance values at one point were obtained from 1994 to 2002 (Rivera, 2004) and four firn cores in the accumulation areas of the Glaciers Moreno (Aristarain and Delmas, 1993), Tyndall (Shiraiwa et al., 2002), Chico (Schwikowski et al., 2006) and PioXI (Schwikowski et al., 2013). In Fig. 3 we compare the results of our simulations to these direct point measurements of the surface mass balance. Satisfactory agreement can be observed between the modeled and the measured data for the ablation data. In the accumulation area, however, in two cases the modeled accumulation is much higher than the observed one. These two point corresponds to firn cores taken on high peaks in the accumulation areas of the Glaciers Perito Moreno and PioXI. The probably large amounts of snow falling at this locations do not persist on the wind-exposed peaks (Schwikowski et al., 2013). Indeed, some ice core drilling sites were specifically chosen to minimize accumulation compared to the surroundings, to obtain longer time series in the shallow ice cores (Schwikowski et al., 2006). The process of wind drift, however, is not incorporated in the model, which likely explains the difference between observed and modeled value. These local effects are important when comparing point measurements with modeled surface mass balance, but should a less important role when estimating the surface mass balance of larger areas as glacier basins or even the entire SPI, since the drifted snow will most probably contribute to the accumulation in another part of the icefield. Since the wind direction is predominately west the snow drift could, however, diminish the accumulation on western windward glacier basins and increase the accumulation on the eastern leeward glacier basins.

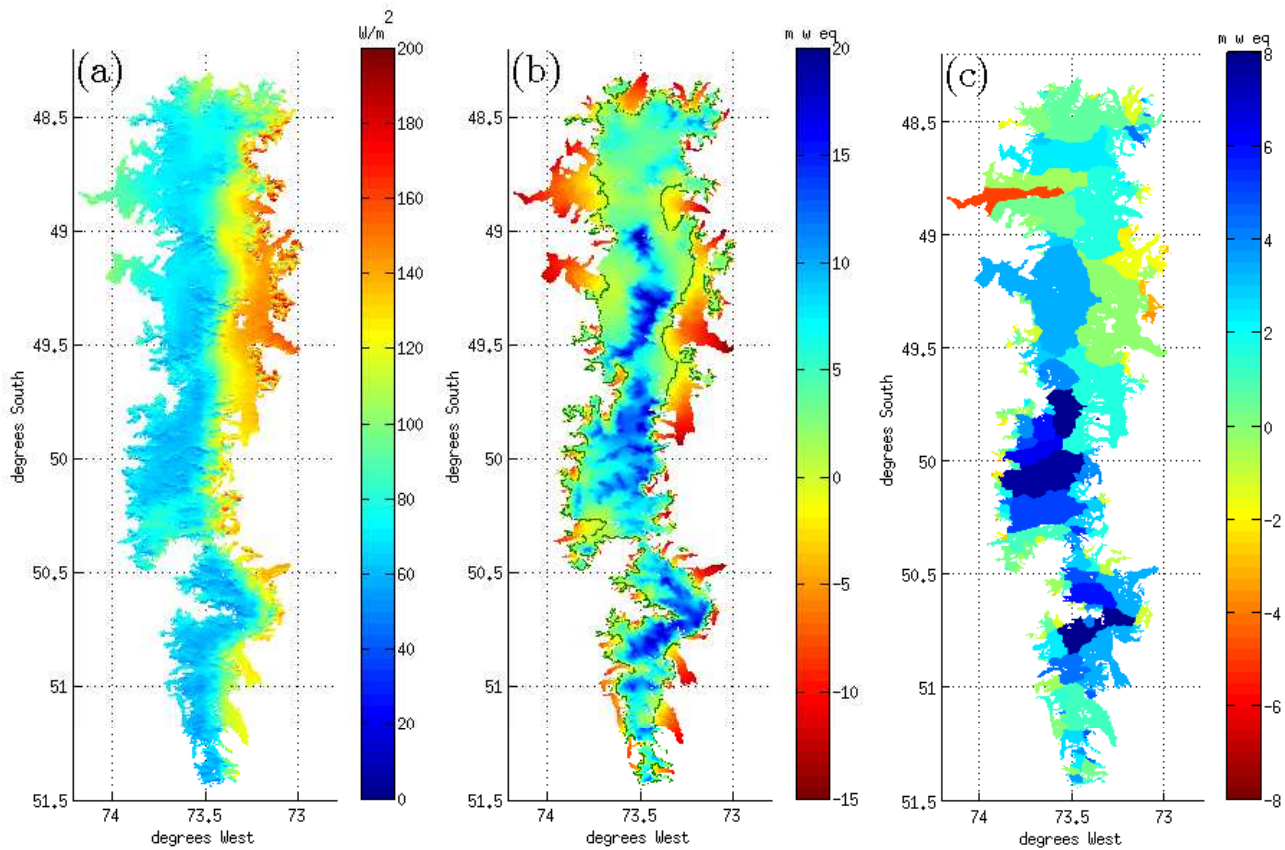


**Fig. 2.** Maps of (a) downscaled incoming solar radiation over SPI; (b) annual surface mass balance of the SPI (green line denotes zero mass balance); (c) annual averaged glacier surface mass balance. All maps show averages 1975-2011.

### 3.3 Evolution of net mass balance values of the SPI

225

The evolution of the annual accumulation, surface ablation and surface mass balance from 1975 to 2010 for the SPI as a whole are presented in Fig. 4. A high inter-annual variability

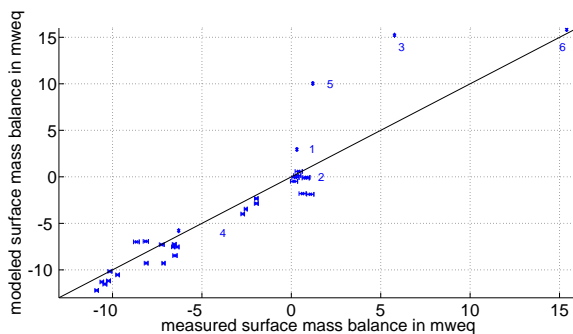


**Fig. 3.** Comparison between measured and simulated surface mass balance: labels correspond to places marked in Fig. 1. The values in the accumulation area are yearly accumulation values, whilst the ablation data are summer, winter or yearly values depending on the availability of data. The uncertainties of the measurements are indicated as error bars in the x direction if available.

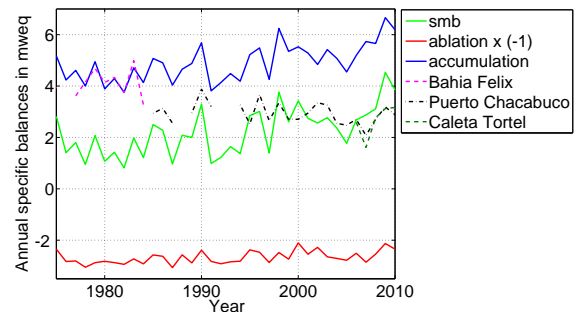


**Fig. 4.** Annual specific accumulation, ablation and surface mass balance (smb) averaged over the SPI from 1975-2010 and yearly measured precipitation sums for selected weather stations in the region: Bahia Felix ( $52^{\circ}58'S, 74^{\circ}08'W$ ) south of the SPI, Puerto Chacabuco ( $45^{\circ}26'S, 72^{\circ}49'W$ ) north of the NPI and Caleta Tortel ( $47^{\circ}47'S, 73^{\circ}32'W$ ) between NPI and SPI.

and an increasing overall trend ( $0.054 \pm 0.012$  mweq/year<sup>2</sup>) of the surface mass balance can be observed. Both the variability and the increasing trend is determined by the accumulation. Furthermore, maxima in accumulation (e.g. 1990, 1998, 2009) are accompanied by minima in ablation, since the higher amounts of snow present in these years reduces the albedo of SPI surface. The variation of measured yearly precipitation at the selected stations in Fig. 4, is similar to the variation of the modeled accumulation. This is a good confirmation of the model's results, considering that measured precipitation data are no direct input data of the model. The average specific melt on the SPI in 1975-2011 is 2.63 mweq/year and the average specific accumulation 4.87 mweq/year. The percentage of solid precipitation of the overall precipitation was 59%, which leads to an average of 8.36 m of yearly precipitation over the SPI for 1975-2011. This value is 19% higher than the 7 m inferred by Escobar et al. (1992), analyzing water discharge data from the 1960s to the 1980s. The higher average precipitation over the SPI obtained by our model can be explained by the increase of accumulation (caused by an increase of precipitation) in the 2000s (Fig. 4). The average modeled precipitation over SPI is slightly higher than the value of 8.03 m modeled for the NPI (Schaefer et al., 2013). It is expected that the total amount of precipitation over the SPI is higher than on the NPI, since wind speeds, which correlate strongly with precipitation in this region, increase to the South (Garreaud et al., 2012; Lenaerts et al., 2014).

When analyzing another important component of the mass balance of the SPI, namely mass losses due to calving, we will transform the modeled mass losses to losses in volume of ice. We can convert the modeled specific mass changes due to surface processes to changes of volume in ice  $\Delta V_{\text{surf}}$  by multiplying with the surface area of the SPI and dividing by the density of ice ( $900 \text{ kg/m}^3$ ). Knowing the total volume change  $\Delta V_{\text{total}}$  of the SPI from geodetic mass balance surveys (Rignot et al., 2003; Willis et al., 2012b), we can calculate the calving losses from the SPI according to:

$$Q_c = \Delta V_{\text{surf}} - \Delta V_{\text{total}}. \quad (1)$$

In 1975-2000 we obtain an increase of ice volume due to surface processes of  $27.7 \text{ km}^3/\text{year}$ . Together with the observed volume loss of  $16.7 \pm 0.9 \text{ km}^3/\text{year}$  observed for this period by Rignot et al. (2003), we obtain calving losses of  $Q_c = 44.4 \text{ km}^3/\text{year}$ . For 2000-2011 we obtain from the observed volume loss of  $21.2 \pm 0.4 \text{ km}^3/\text{year}$  (Willis et al., 2012b) and the modeled increase in volume due to surface processes of  $40.1 \text{ km}^3/\text{year}$  calving losses of  $Q_c = 61.3 \text{ km}^3/\text{year}$ . The uncertainties associated with these inferred calving fluxes from the SPI are high. It is difficult to a priori constrain the uncertainties associated with the modeled ice volume change due to surface mass balance (see section 3.5) and we therefore try to learn about these uncertainties by comparing inferred calving fluxes to calving fluxes estimated from velocity measurements at the different

glacier catchments (section 3.6, Table 1). Also the uncertainties associated with the geodetic balances might be higher than stated by their authors: both authors of the geodetic balances assume that all volume change is due to ice loss and therefore convert volume loss to mass loss assuming a density of  $900 \text{ kg/m}^3$ . Willis et al. (2012b) details volume loss for ablation area and accumulation separately. If we assume that the volume loss in the accumulation area is due melt of firm with a density of  $550 \text{ kg/m}^3$ , the corresponding ice loss would be lower and the calving fluxes would lower to  $Q_c = 56.8 \text{ km}^3/\text{year}$ . Although assuming large uncertainties on the inferred overall calving losses of SPI, we can still state that a strong increase in calving losses took place, which is motivated by an acceleration of the glaciers of SPI (Jaber et al., 2012; Rivera et al., 2012a; Sakakibara et al., 2013). For comparison, the modeled yearly accumulation over the SPI for 1975-2000 corresponds to  $66.7 \text{ km}^3$  of ice per year and  $73.1 \text{ km}^3$  of ice per year for 2000-2011 and the modeled melt from SPI is  $39.0 \text{ km}^3/\text{year}$  for 1975-2000 and  $33.0 \text{ km}^3/\text{year}$  for 2000-2011. This means that the inferred losses due to calving are higher than losses by melt in both periods. In all these conversions we used the SPI reference area of  $13000 \text{ km}^2$  from Rignot et al. (2003) to convert the specific values to overall change for 1975-2000 and the area of  $12100 \text{ km}^2$  (Willis et al., 2012b) for 2000-2011.

### 3.4 Surface mass balance of the individual glacier catchments

Apart from the overall trend in the mass balance components of the SPI, it is interesting to analyze the individual glacier catchments as closed systems, to be able to quantify the different contributions of the terms of the mass balance for the different glaciers. However, due to the large flat areas on the SPI, the definition of the catchments (especially in the northern part of the SPI) is not unique and probably also changing through time (Rivera et al., 2012a). In Fig 2c we present the 1975-2011 average specific annual surface mass balance of the individual glaciers using the catchments defined in the Randolph Glacier Inventory (RGI) (Arendt, 2012). In the northern part of the SPI (north of  $49.5^\circ \text{S}$ ) the main glaciers have annual glacier surface mass balances ranging from slightly negative (Chico Glacier  $-1.58$  mweq) to clearly positive (PioXI Glacier  $3.45$  mweq). The only exception is Occidental Glacier having a clearly negative annual surface mass balance ( $-4.85$  mweq). Since this glacier does not show an exceptional retreat or thinning behavior (López et al., 2010; Willis et al., 2012b), we think that the exceptionally negative glacier surface mass balance is caused by an erroneous delineation of glacier catchments where parts of the glacier's accumulation area were considered as belonging to neighboring glaciers. The Glacier PioXI has the most positive annual surface mass balance in the area, which agrees with the advance of the glacier observed until recently (Rivera et al., 1997). In the middle-southern part of

the SPI (between 49.5°S and 50.5°S), the annual surface  
 325 mass balance of the western glaciers are very positive (up  
 to 10.0 mweq for Glacier HPS13) and moderately positive  
 for the eastern glaciers. The very positive modeled surface  
 330 mass balance of the western glaciers agrees with the accumu-  
 lation area ratios of  $>0.8$  observed at these glaciers (Aniya  
 et al., 1996; Casassa et al., 2013). At the periphery of the  
 SPI several small glaciers can be spotted in Fig 2c which of-  
 ten exhibit negative surface mass balance, which is in good  
 agreement with the high relative area loss observed at these  
 glaciers (Davies and Glasser, 2012). 385

A characteristic parameter of a glacier is the altitude at  
 which accumulation and ablation are of same magnitude, the  
 Equilibrium Line Altitude (ELA). We present 1975-2011 av-  
 eraged ELAs computed by the model in Table 1. For compar-  
 340 ison we also present the average snow line altitude (SLA) 390  
 at the end of the summers 2002 and 2004 computed recently  
 by De Angelis (2014). For several glaciers (Amalia, Europa,  
 Grey, HPS15, HPS19, HPS31, Penguin, Perito Moreno) the  
 model ELAs agree with the average SLA at the end of the  
 summers 2002 and 2004 within two sigmas. At the glaciers 395  
 Asia, BGOT, CV, O'Higgins, PioXI, Upsala and Jorge Montt  
 the average model ELA is higher than the average SLA at  
 the end of the summers 2002 and 2004. This discrepancy  
 can be explained by the possibility of snowfalls before the  
 acquisition of the examined satellite images and by the high  
 345 inter-annual variability of the surface mass balance (Fig. 4).  
 This idea is supported by the observation of a SLA at the end  
 of the summer 1986 of 1300 m at O'Higgins Glacier (Aniya  
 et al., 1996), which is even higher than the model average  
 ELA. The model ELAs are considerably lower than the av-  
 350 erage SLA at the end of the summers 2002 and 2004 for the  
 glaciers HPS12, HPS13, HPS29 and HPS34. This could also  
 be due to the inter-annual variability of the surface mass bal-  
 ance, however since the SLA at the end of the summer rather  
 tends to underestimate the ELA than to overestimate it (due  
 360 to possible snowfalls on the SPI during the whole year), this  
 could also indicate a local overestimation of the surface mass  
 balance by the model at these glaciers. At HPS34 the SLA at  
 the end of the summer 1986 of 900 m (Aniya et al., 1996),  
 agrees much better with the average model ELA than the  
 365 SLA computed by De Angelis (2014).

### 3.5 Sources of uncertainties for the modeled surface mass balance

We want to point out that our surface mass balance model-  
 370 ing approach is subject to different uncertainties, which are  
 difficult to quantify in a systematic way. Several reanalysis  
 datasets were suspected to have spurious increases in precipi-  
 tation at high Southern latitudes due to the inclusions of new  
 375 datasets (Nicolas and Bromwich, 2011). Regional climate  
 models still have problems to correctly quantify orographic  
 precipitation, which was the reason for the fact that we had  
 to apply a global correction factor to the precipitation data

(Schaefer et al., 2013). This factor could vary spatially and  
 temporally. Also no direct air temperature data from the ice-  
 field itself were available to validate the modeled tempera-  
 tures. The acquisition of climate data on the icefield itself  
 would be very valuable to be able to better constrain the un-  
 certainties of the model results.

### 3.6 Calving losses of the individual glaciers

Additionally to mass losses due to surface melt, nearly all  
 major outlet glaciers of the SPI have additional mass losses  
 due to calving (Warren and Aniya, 1999), which makes the  
 total mass balance of the glaciers negative. Calving fluxes  $Q_c$   
 can be inferred for the individual catchments using equation  
 (1) again. In Table 1 we present the inferred calving fluxes  
 in 1975-2000 and 2000-2011 for the most important outlet  
 glaciers of the SPI. Since the ice divides in the flat parts of  
 the SPI are difficult to determine, in Table 1 we present the  
 Glaciers Bernardo, Greve, Occidental and Tempano in the  
 north of the SPI as one glacier (BGOT). We did the same for  
 the glaciers Chico and Viedma (CV) which share the glacier  
 plain around the Paso de los Cuatro Glaciares. The errors  
 indicated for the inferred calving fluxes presented in Table 1  
 are the inherited (quantifiable) uncertainties of the geodetic  
 measurements. They should not be interpreted as the total  
 uncertainty of the inferred fluxes, since the (unknown) un-  
 certainties of the model results are not included. For calving  
 fluxes inferred for 2000-2011, we present a range, which is  
 obtained by converting the volume loss in the accumulation  
 area detected by Willis et al. (2012b) to mass loss using the  
 density of firn (550 kg/m<sup>3</sup>) as lower limit and the density of  
 ice (900 kg/m<sup>3</sup>) as upper limit.

To validate the inferred calving fluxes, we computed calv-  
 ing fluxes from a complete velocity field of the SPI obtained  
 from a speckle-tracking analysis of RADARSAT-1 images  
 from September 2004 to November 2004. For every glacier  
 we computed the average velocity at the front  $\bar{V}$  and derived  
 calving flux from the width at the front  $W$ ,  $\bar{V}$  and the aver-  
 age ice thickness at the front  $\bar{H}$ . The latter, however, was  
 mostly unknown. Bathymetric measurements of the water  
 bodies in which the glaciers are calving were available for  
 the glaciers Jorge Montt (Rivera et al., 2012b), O'Higgins  
 (unpublished data), Perito Moreno (Rott et al., 1998), Up-  
 sala (Skvarca et al., 2003), PioXI (Warren and Rivera, 1994)  
 and Tyndall (Raymond et al., 2005), which provided a good  
 constraint to the ice thickness at the front. There exist bathy-  
 metric measurements from Chilean Navy Hydrographic and  
 Oceanographic Service (SHOA) in many Patagonian fjords  
 as well, but mostly they are not extending towards the glacier  
 fronts. In Fig. 1 we present some point measurements from  
 SHOA. Therefore, for most of the other glaciers, an ice thick-  
 ness of  $300 \pm 250$  m was assumed, which means that we as-  
 sign a 68% probability to the event that at an arbitrary calving  
 glacier tongue of the SPI has an ice thickness between 50 and  
 550 meters. This is motivated by our experience that calving

Glacier	ELA (m)	SLA (m)	$Q_c$ Inferred	$Q_c$ Inferred	$Q_c$ From velocities	$W_{tot}$ (km)	$\bar{V}$ (km/year)	$\bar{H}$ (m)	Agreement within $1\sigma$
	1975-2011	DeAngelis2014	1975-2000 (km <sup>3</sup> /year)	2000-2011 (km <sup>3</sup> /year)	Spring 2004 (km <sup>3</sup> /year)				
Amalia	861	930±40	0.78±0.05	(0.92-0.96)±0.07	0.42±0.35	2.45	0.57	300±250	R
Asia	918	800±20	0.32±0.03	(0.48-0.50)±0.05	0.26±0.21	0.85	1.00	300±250	RW
BGOT	1068	945±30	1.54±0.18	(1.72-2.12)±0.18	1.80±1.03	12.51	0.48	300±250	RW
CV	1438	1264±24	-1.00±0.24	(1.86-2.25)±0.09	0.36±0.30	1.97	0.41	230±180	-
Europa	995	940±30	no data	(2.75-2.81)±0.08	0.41±0.34	0.92	1.48*	300±250	-
Grey	1021	980±50	1.33±0.05	(1.51-1.55)±0.10	0.39±0.32	2.17	0.47	300±250	-
HPS12	983	1150±30	no data	(1.38-1.43)±0.05	0.55±0.46	0.80	2.29*	300±250	-
HPS13	967	1140±60	no data	(1.37-1.38)±0.04	1.07±0.89	0.94	3.80*	300±250	W
HPS15	928	950±50	no data	(0.85-0.88)±0.04	0.55±0.46	0.92	2.00*	300±250	W
HPS19	981	1070±60	no data	(1.37-1.42)±0.06	0.43±0.36	0.75	1.93*	300±250	-
HPS29	951	1170±70	0.47±0.02	(0.57-0.60)±0.05	0.52±0.43	1.22	1.41	300±250	RW
HPS31	951	990±51	1.07±0.03	(1.04-1.08)±0.06	0.41±0.34	0.75	1.80*	300±250	-
HPS34	869	1240±100	1.32±0.03	(1.66-1.72)±0.06	0.85±0.71	1.89	1.50*	300±250	RW
Jorge Montt	1112	930±40	1.96±0.10	(1.43-1.58)±0.06	1.20±0.54	2.10	2.59	220±50	W
O'Higgins	1282	1200±20	2.15±0.15	(2.97-3.27)±0.13	1.78±0.52	2.33	2.25	340±100	R
Penguin	955	1070±70	no data	(4.61-4.72)±0.08	0.83±0.69	1.20	2.30*	300±250	-
Perito Moreno	1150	1230±40	0.99±0.04	(1.44-1.57)±0.08	0.44±0.16	4.90	0.65	140±50	-
Pro XI	1055	930±50	3.69±0.32	(5.99-6.35)±0.14	2.69±1.71	9.82	1.74*	200±100	R
Tyndall	899	940±10	0.83±0.06	(1.58-1.69)±0.11	0.14±0.08	2.28	0.35	181±100	-
Upsala	1249	1170±30	1.75±0.17	(4.67-5.05)±0.08	2.41±0.40	2.64	1.52	540±100	R

**Table 1.** 1975-2011 average altitude of zero surface mass balance (ELA) computed by the model and the average altitude of the snow line at the end of the summers 2002 and 2004 computed by De Angelis (2014) (columns 1+2). Inferred calving fluxes according to eq. (1) using the geodetic mass balance measurements of Rignot et al. (2003) for the period 1975-2000 and of Willis et al. (2012a) for 2000-2011 (column 3+4). Calving fluxes based on a velocity-map from spring 2004 (column 5) and explicit data used to compute these fluxes (columns 6 to 8). The star marks the velocity data that were taken from a point farther than 1 km upstream of the glacier front. Column 8 indicates if the calving fluxes computed from the velocity field agree within one standard deviation with the inferred fluxes for 1975-2000 (R) or 2000-2011 (W) or both (RW).

glaciers of similar size have normally ice cliffs of 50 m and larger and are normally not able to persist in water bodies of depth greater than 500 m. For Chico Glacier we estimated  $\bar{H}=100\pm 50$  m. Calving fluxes were computed according to  $Q_c = \bar{V} \cdot \bar{H} \cdot W$ , where the products were obtained for every tongue and summed up in the case of several tongues (BGOT for example). The obtained calving fluxes, together with the explicit data for mean velocity, tongue width and estimated ice thickness are presented in Table 1 as well. The uncertainties of the calving fluxes estimated from the velocity field are dominated by the uncertainties of the ice thickness.

The comparison of the inferred calving fluxes with the calving fluxes computed from the velocity field in spring 2004 shows that the inferred calving fluxes are systematically higher. One immediate explanation for this is the fact that at the glacier fronts the method of speckle-tracking analysis of RADARSAT-1 images does not work very well due to loss of coherence induced by fast ice deformation which changes the characteristic patterns of the glacier over the 24 day cycles of the satellite. Therefore the data presented in Table 1 do not always correspond to the glacier's velocity right at the glacier front. Since calving glaciers normally show high shear rates at the glacier fronts (for example San Rafael Glacier, Willis et al. (2012a)), this leads to an underestimation of the calving flux. This might explain the discrepancy between inferred calving fluxes and the calving fluxes estimated from the velocity measurements for the glaciers Europa, HPS12, HPS19 and Penguin, where clearly higher velocity have been registered for the period 2005-2011 using cross-correlation techniques with satellite images (private communication with M. Willis, September 2014).

Not very coherent data on calving fluxes could be inferred for the CV glacier complex. In 1975-2000 Rignot et al. (2003) detected very low thinning ( $0.01\pm 0.25$  mweq), whilst the model is producing a negative glacier surface balance, which produces the negative calving fluxes. We think that in this case Rignot et al. (2003) is underestimating the thinning of the glacier, since it contradicts the considerable area loss and retreat of the glacier detected during 1986-2001 (Davies and Glasser, 2012; White and Copland, 2013). Here it has to be noted that the annual balances for Argentinian glaciers in Rignot et al. (2003) are in reality averages over the period 1968-2000 and that the digital elevation model generated for the Argentinian glaciers in 1968 has a much lower precision than the digital elevation model of Chilean glaciers from 1975. On the other hand, the high thinning observed in 2000-2011 seems to disagree with the moderate calving estimated from the velocity data. However newer velocity data from Viedma Glacier (Riveros et al., 2013) indicate front velocities three times higher than our data, which would bring the calving flux estimation in better agreement with the inferred fluxes for 2000-2011.

For the glaciers Moreno, Grey and Tyndall the velocity data from the speckle-tracking analysis of RADARSAT-1 images are available at the front of the glaciers. And for Perito Moreno Glacier similar velocity data were obtained before and after 2004 (Rott et al., 1998; Ciappa et al., 2010). Still, the inferred calving fluxes are much higher than the ones estimated from the velocity data. According to eq. (1), this disagreement could be due to a local overestimation of the modeled surface mass balance or an overestimation of the volume losses by the geodetic mass balances. Since the thin-

ning observed in the geodetic mass balances (Rignot et al., 2003; Willis et al., 2012b) at Glacier Perito Moreno con-  
 495 tradicts its stable behavior with even some advances observed during the end of the 20th century and the beginning of the  
 21st century, we computed calving fluxes assuming a total glacier mass balance of zero at Perito Moreno Glacier. In  
 this case we would obtain  $Q_c=0.78 \text{ km}^3/\text{year}$  for 1975-2000 and  $Q_c=1.10 \text{ km}^3/\text{year}$  for 2000-2011. These inferred cal-  
 500 v-530 ing fluxes are still clearly higher than the ones estimated from velocity data and we therefore examine the modeled surface  
 mass balance at Perito Moreno Glacier in more detail.

### 3.7 Mass balance of the Perito Moreno Glacier

In Fig. 5 we present the modeled 1975-2011 average specific surface mass balance as it varies with altitude. In the

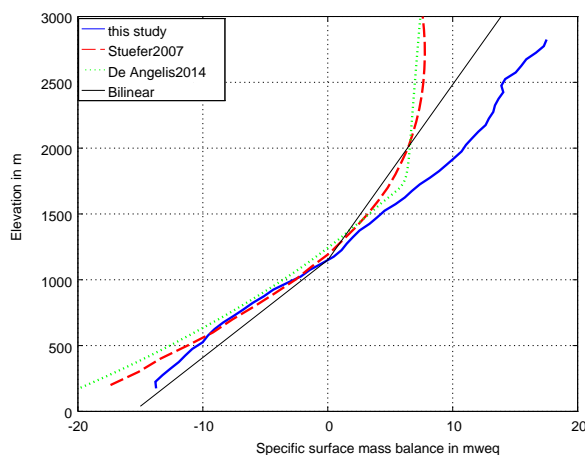


**Fig. 5.** Specific surface mass balance profiles for Perito Moreno Glacier obtained from this study (blue), Stuefer et al. (2007) (red-dashed) and De Angelis (2014) (green dotted). Theoretical bilinear profile for comparison.

505 same graph, we present the specific surface mass balance profile obtained by Stuefer et al. (2007) for the balance year  
 1999/2000 using a degree-day-model calibrated with stake measurements in the ablation zone between 1995 and 2003  
 and precipitation data from a precipitation climatology which was extrapolated to the glacier assuming a linear precipita-  
 510 tion increase below the ELA and a precipitation increase determined by a curve which asymptotically approached a maximum  
 precipitation value at an elevation of 2500 m above the ELA. This maximum precipitation value was adjusted  
 515 to gain an overall mass balance of zero of the glacier. Furthermore we show the specific surface mass balance profile  
 obtained by De Angelis (2014) using a degree day model for ablation as well and stochastically modeled precipitation  
 520 which was also constrained by an inferred total accumulation value. Furthermore we show a bilinear profile obtained by  
 assuming a constant specific surface mass balance gradient of

0.0135 mweq/m in the ablation zone and of 0.0075 mweq/m in the accumulation zone. The profiles agree relatively well  
 in the ablation zone with the profile of De Angelis (2014) and Stuefer et al. (2007) having slightly lower specific surface  
 mass balance at lower elevations. In the accumulation zone, the profiles show strong differences. Stuefer et al. (2007) assume  
 an upper limit 7.6 m of precipitation which constrains the accumulation above 2500 m elevation. De Angelis (2014)  
 obtains a very pronounced kink in the specific surface mass balance profile at an elevation of 1700 m. The bilinear profile,  
 by definition, has a kink at the ELA, whilst in our modeled profile the specific surface mass balance continues to in-  
 535 crease with altitude in the accumulation area at a similar rate as in the ablation area. The consequence of this strong in-  
 crease is a very high specific surface mass balance of around 17.5 mweq at an elevation of 2800 m. This high gradient of  
 the surface mass balance in the accumulation area is producing an elevated surface mass balance for the entire glacier  
 which causes the overestimation of the calving fluxes when applying equation (1). Since the accumulation which de-  
 540 termines the specific surface mass balance profile above the ELA, was tuned by the other two authors to match the over-  
 all observed zero mass balance of the glacier, their profiles probably quantify better the surface mass balance at higher  
 altitudes. However without having spatially distributed accumulation measurements at our disposal we can not judge  
 which of the specific surface mass balance profiles quantifies best the accumulation on the Perito Moreno Glacier.

550 Another explanation for a local overestimation of the calving fluxes computed by eq. (1) could be the existence of an  
 additional process of mass loss which is not accounted for in the equation. Since there are four active volcanoes that coin-  
 555 cide with the Southern part of the SPI (see Fig. 1), volcanic activity could induce sub-glacial melt which would lower the  
 mass balance of the glaciers and possibly explain the discrepancy between inferred calving fluxes and measured ones.  
 However, assuming a high constant geothermal heat flow of  $1000 \text{ mW/m}^2$  (mean heat flow over the continental crust is  
 $65 \text{ mW/m}^2$ ), would only lower the specific mass balance by  $0.09 \text{ m w eq}$ . On a glacier like Perito Moreno for example this  
 would only cause an additional mass loss of  $0.03 \text{ km}^3$ , a very low value compared to the high mass turn-over of the glacier  
 and the large uncertainties concerning the calving fluxes.

## 4 Conclusions

In this contribution we present a first quantification of mass balance processes for the Southern Patagonia Icefield. We  
 conclude that the surface mass balance of the SPI is positive and that it was increasing during 1975-2011. The increase  
 and the variability of the modeled surface mass balance was determined by the accumulation which was  $67.7 \text{ km}^3$  of ice  
 per year on average in 1975-2011. The modeled average surface melt was  $36.5 \text{ km}^3$  of ice per year and showed good

agreement with sparse data from stakes. Using overall bal-  
 575 ances from geodetic mass balance surveys, calving fluxes  
 could be inferred from the modeled surface mass balance.  
 The inferred losses due to calving showed a strong increase  
 580 from 44.4 km<sup>3</sup> (1975–2000) to 61.3 km<sup>3</sup> ice per year (2000–  
 2011). In both cases they were higher than losses due to  
 melt of snow and ice (39 km<sup>3</sup> of ice per year for 1975–2000  
 and 33 km<sup>3</sup> for 2000–2011). Since the uncertainties of sur-  
 face mass balance due to the scarcity of validation data are  
 difficult to constrain, the uncertainties of these numbers are  
 585 relatively high. Additionally, geodetic mass balance surveys  
 are subject to important uncertainties, because of the often  
 unknown density in the accumulation area of the glaciers.  
 Assigning a density of 550 kg/m<sup>3</sup> (instead of 900 kg/m<sup>3</sup>) to  
 the mass loss in the accumulation area of SPI, for exam-  
 590 ple, would lower the inferred calving fluxes in 2000–2011  
 to 56.8 km<sup>3</sup>/year.

Comparison of the inferred calving fluxes of the most im-  
 600 portant outlet glaciers with calving fluxes estimated from a  
 velocity field obtained in spring 2004, showed satisfactory  
 agreement for several glaciers. However, the uncertainties of  
 595 the calving fluxes estimated from the velocity data are large,  
 due to the mostly unknown ice thickness at the glaciers' fronts.  
 On some glaciers the inferred calving fluxes overestimate  
 the losses due to calving. Therefore, the inferred over-  
 all calving fluxes should be better interpreted as an upper-  
 605 boundary-estimate.

Long-term velocity measurements and ice-thickness mea-  
 610 surements at the calving front of the glaciers are necessary  
 to better constrain the calving losses from the SPI, which  
 would help significantly to reduce the uncertainties of sur-  
 face mass balance reconstructions as well. Ablation mea-  
 615 surements at more glaciers (especially at the western side of  
 the SPI) could help to better judge the performance of sur-  
 face mass balance models on the SPI. Since precipitation is  
 one of the most insecure output of regional climate models,  
 620 spatially distributed accumulation measurements could help  
 to better judge the performance of these models. Appropriate  
 sites for accumulation measurements are smooth and rather  
 flat areas in the central plateau of the accumulation area of  
 625 the glaciers at elevations of about 1500 m.a.s.l. and not wind  
 exposed peaks and ridges where snow drift is dominating the  
 accumulation patterns.

## 5 Acknowledgments

The authors would like to thank the Chilean Weather Service  
 630 (DMC) and the Chilean Water Directory (DGA) for provid-  
 ing meteorological data, Andres Rivera for sharing the data  
 of his PhD-thesis, Mike Willis for sharing the glacier out-  
 lines used in his work and anticipating his unpublished veloc-  
 ity data, Hernán De Angelis and Martin Stuefer for sharing  
 635 their mass balance profile data electronically and the Chilean  
 Navy Hydrographic and Oceanographic Service (SHOA) for

providing bathymetric data for the Patagonian fjords. M.  
 Schaefer is FONDECYT Postdoc Fellow (project number  
 3140135). This work was partly supported by funding from  
 the ice2sea programme from the European Union 7th Frame-  
 work Programme, grant number 226375. Ice2sea contribu-  
 tion number 168.

## References

- Aniya, M., Sato, H., Naruse, R., Skvarca, P., and Casassa, G.:  
 The Use of Satellite and Airborne Imagery to Inventory Outlet  
 Glaciers of the Southern Patagonia Icefield, South America, *Pho-  
 togrammetric Engineering and Remote Sensing*, 62, 1361–1369,  
 1996.
- Aravena, J.-C. and Luckman, B. H.: Spatio-temporal rainfall pat-  
 terns in Southern South America, *International Journal of Cli-  
 matology*, 29, 2106–2120, doi:10.1002/joc.1761, 2009.
- Arendt, e. a.: Randolph Glacier Inventory [v3.0]: A Dataset of  
 Global Glacier Outlines, Tech. rep., Global Land Ice Measure-  
 ments from Space, Boulder Colorado, USA, 2012.
- Aristarain, A. and Delmas, R.: Firn-core study from the Southern  
 Patagonia Ice Cap, South America, *Journal of Glaciology*, 39,  
 249–254, 1993.
- Carrasco, J., Casassa, G., and Rivera, A.: Meteorological and Cli-  
 matological aspects of the Southern Patagonia Icefield, in: *The  
 Patagonian Icefields A Unique Natural Laboratory for environ-  
 mental and Climate Change Studies*, p. 29–41, 2002.
- Casassa, G., Rodríguez, J. L., and Loriaux, T.: A new glacier in-  
 ventory for the Southern Patagonia Icefield and areal changes  
 1986–2000, Chapter 27 in *Global Land Ice Measurements from  
 Space*, Springer Praxis Books, 2013.
- Ciappa, A., Pietranera, L., and Battazza, F.: Perito Moreno Glacier  
 (Argentina) flow estimation by COSMO SkyMed sequence of  
 high-resolution SAR-X imagery, *Remote Sensing of Environ-  
 ment*, 114, 2088–2096, 2010.
- Corripio, J.: Vectorial algebra algorithms for calculating terrain pa-  
 rameters from DEMs and solar radiation modelling in mountain-  
 ous terrain, *International Journal of Geographical Information  
 Science*, 17, 1–23, doi:10.1080/713811744, 2003.
- Davies, B. J. and Glasser, N.: Accelerating shrinkage of Patagonian  
 glaciers from the Little Ice Age ( AD1870) to 2011, *Journal of  
 Glaciology*, 58, 1063–1084, doi:10.3189/2012JoG12J026, 2012.
- De Angelis, H.: Hypsometry and sensitivity of the mass balance  
 to changes in equilibrium-line altitude: the case of the Southern  
 Patagonia Icefield, *Journal of Glaciology*, 60, 14–28, 2014.
- 670 Escobar, F., Vidal, F., Garin, C., and Naruse, R.: Water balance in  
 the Patagonia Icefield, Tech. rep., Institute of Low Temperature  
 Research, 1992.
- Falvey, M. and Garreaud, R. D.: Regional cooling in a warm-  
 ing world: Recent temperature trends in the southeast Pacific  
 and along the west coast of subtropical South America (1979–  
 2006), *Journal of Geophysical Research*, 114, doi:10.1029/  
 2008JD010519, 2009.
- Fowler, H. J., Blenkinsop, and Tebaldib, C.: Linking climate  
 change modelling to impacts studies: recent advances in down-  
 scaling techniques for hydrological modelling, *International  
 Journal of Climatology*, 27, 1547–1578, 2007.

- Garreaud, R. and Lopez, P., Minvielle, M., and Rojas, M.: Large Scale Control on the Patagonia Climate, *Journal of Climate*, 26, 215–230, 2012.
- 685 Ibarzabal y Donangelo, T., Hoffmann, J., and Naruse, R.: Recent climate changes in southern Patagonia, *Bulletin of Glacier Research*, 14, 29–36, 1996.
- Jaber, W. A., Floricioiu, D., Rott, H., and Eineder, M.: Dynamics of fast glaciers in the Patagonia Icefields derived from Terrasar-X and Tandem-X data, in: *Geoscience and Remote Sensing Symposium (IGARSS), 2012 IEEE International*, 2012. 690
- Kalnay, E., Kanamitsu, M., Kistler, R., Collins, W., Deaven, D., Gandin, L., Iredell, M., Saha, S., White, G., Woollen, J., Zhu, Y., Chelliah, M., Ebisuzaki, W., Higgins, W., Janowiak, J., Mo, K., Ropelewski, C., Wang, J., Leetmaa, A., Reynolds, R., Jenne, R., and Joseph, D.: The NCEP/NCAR 40-year reanalysis project, *Bulletin of the American Meteorological Society*, 77, 437–471, doi:10.1175/1520-0477(1996)077<0437:TNYRP>2.0.CO;2, 1996.
- 700 Lenaerts, J. T. M., van den Broeke, M. R., van Wessem, J. M., van de Berg, W. J., van Meijgaard, E., van Uft Lambertus H, and Schaefer, M.: Extreme precipitation and climate gradients in Patagonia revealed by high-resolution regional atmospheric climate modelling, *Journal of Climate*, accepted for publication, 2014. 705
- López, P., Chevallier, P., Favier, V., Pouyaud, B., Ordenes, F., and Oerlemans, J.: A regional view of fluctuations in glacier length in southern South America, *Global and Planetary Change*, 71, 85–108, 2010.
- 710 Machguth, H., Paul, F., Kotlarski, S., and Hoelzle, M.: Calculating distributed glacier mass balance for the Swiss Alps from regional climate model output: A methodical description and interpretation of the results, *Journal of Geophysical Research-Atmospheres*, 114, doi:10.1029/2009JD011775, 2009.
- 715 Masiokas, M. H., Rivera, A., Espizua, L. E., Villalba, R., Delgado, S., and Carlos Aravena, J.: Glacier fluctuations in extratropical South America during the past 1000 years, *Palaeogeography Palaeoclimatology Palaeoecology*, 281, 242–268, doi:10.1016/j.palaeo.2009.08.006, 2009.
- 720 Nicolas, J. and Bromwich, D.: Precipitation Changes in High Southern Latitudes from Global Reanalyses: A Cautionary Tale, *Surv Geophys*, 32, 475–494, 2011.
- Oerlemans, J.: *Glaciers and Climate Change*, A.A. Balkema Publishers, 2001.
- 725 Orihashi, Y., Naranjo, J., Motoki, A., Sumino, H., Hirata, D., Anma, R., and Nagao, K.: The Quaternary volcanic activity of Hudson and Lautaro volcanoes, Chilean Patagonia: new age constraints from K-Ar ages, *Revista Geológica de Chile*, 31, 207–224, 2004.
- Rasmussen, L. A., Conway, H., and Raymond, C. F.: Influence of upper air conditions on the Patagonia icefields, *Global and Planetary Change*, 59, 203–216, doi:10.1016/j.gloplacha.2006.11.025, 730 2007.
- Raymond, C., Neumann, T., Rignot, E., Echelmeyer, K., Rivera, A., and Casassa, G.: Retreat of Glacier Tyndall, Patagonia, over the last half-century, *Journal of Glaciology*, 51, 239–247, doi:10.3189/172756505781829476, 2005. 735
- Rignot, E., Rivera, A., and Casassa, G.: Contribution of the Patagonia Icefields of South America to sea level rise, *Science*, 302, 434–437, doi:10.1126/science.1087393, 2003.
- 740 Rivera, A.: Mass balance investigations at Glacier Chico, Southern Patagonia Icefield, Chile, Ph.D. thesis, University of Bristol, 2004.
- Rivera, A., Lange, H., Aravena, J., and Casassa, G.: The 20th-century advance of Glacier Pio XI, Chilean Patagonia, in: *Annals of Glaciology*, Vol 24, 1997, pp. 66–71, 1997.
- Rivera, A., Corripio, J., Bravo, C., and Cisternas, S.: Glacier Jorge Montt (Chilean Patagonia) dynamics derived from photos obtained by fixed camera and satellite image feature tracking, *Annals of Glaciology*, 53, 147–155, 2012a.
- Rivera, A., Koppes, M., Bravo, C., and Aravena, J.: Little Ice Age advance and retreat of Glacier Jorge Montt, Chilean Patagonia, *Climate of the Past*, 8, 403–414, 2012b.
- Riveros, N., Euillades, L., Euillades, P., Moreiras, S., and Balbarani, S.: Offset tracking procedure applied to high resolution SAR data on Viedma Glacier, Patagonian Andes, Argentina, *Advances in Geosciences*, 35, 7–13, doi:10.5194/adgeo-35-7-2013, 2013.
- Rosenblüth, B., Casassa, G., and Fuenzalida, H.: Recent climatic changes in western Patagonia, *Bulletin of Glacier Research*, 13, 127–132, 1995.
- Rott, H., Stuefer, M., Siegel, A., Skvarca, P., and Eckstaller, A.: Mass fluxes and dynamics of Moreno Glacier, Southern Patagonia Icefield, *Geophysical Research Letters*, 25, 1407–1410, doi:10.1029/98GL00833, 1998.
- Sakakibara, D., Suggiyama, S., Sawagaki, T., Marinsek, S., and Skvarca, P.: Rapid retreat, acceleration and thinning of Glacier Upsala, Southern Patagonia Icefield, initiated 2008, *Annals of Glaciology*, 54, 131–138, 2013.
- Schaefer, M., Machguth, H., Falvey, M., and Casassa, G.: Modeling past and future surface mass balance of the Northern Patagonian Icefield, *Journal of Geophysical Research Earth Surface*, 118, 571–588, doi:10.1002/jgrf.20038, 2013.
- Schwikowski, M., Bruetsch, S., Casassa, G., and Rivera, A.: A potential high-elevation ice-core site at Hielo Patagónico Sur, in: *Annals of Glaciology*, VOL 43, 2006, pp. 8–13, doi:10.3189/172756406781812014, 2006.
- Schwikowski, M., Schläppi, M., Santibanez, P., Rivera, A., and Casassa, G.: Net accumulation rates derived from ice core stable isotope records of Pío XI glacier, Southern Patagonia Icefield, *The Cryosphere*, 7, 1635–1644, 2013.
- Shiraiwa, T., Kohshima, S., Uemura, R., Yoshida, N., Matoba, S., Uetake, J., and Godoi, M.: High net accumulation rates at Campo de Hielo Patagónico Sur, South America, revealed by analysis of a 45.97 m long ice core, in: *Annals of Glaciology*, VOL 35, pp. 84–90, doi:10.3189/172756402781816942, 2002.
- Skvarca, P., Raup, B., and De Angelis, H.: Recent behaviour of Glacier Upsala, a fast-flowing calving glacier in Lago Argentino, southern Patagonia, in: *Annals of Glaciology*, Vol 36, edited by Raymond, C., pp. 184–188, doi:10.3189/172756403781816202, 2003.
- Stern, C.: Active Andean volcanism: its geologic and tectonic setting, *Revista Geológica de Chile*, 31, 161–206, 2004.
- Stern, C.: Holocene tephrochronology record of large explosive eruptions in the southernmost Patagonian Andes, *Bull Volcanol*, 70, 435–454, 2008.
- Stuefer, M., Rott, H., and Skvarca, P.: Glacier Perito Moreno, Patagonia: climate sensitivities and glacier characteristics preceding the 2003/04 and 2005/06 damming events, *Journal of Glaciology*, 53, 3–15, 2007.
- Warren, C. and Aniya, M.: The calving glaciers of southern South

800 America, *Global and Planetary Change*, 22, 59–77, doi:10.1016/S0921-8181(99)00026-0, 1999.

Warren, C. and Rivera, A.: Non-linear climatic response of Calving Glaciers: A case study of Pio XI Glacier, Chilean Patagonia, *Revista Chilena de Historia Natural*, 67, 385–394, 1994.

805 White, A. and Copland, L.: Spatial and temporal variations of glacier extent across the Southern Patagonian Icefield since the 1970s, *The Cryosphere Discussions*, 7, 1–34, 2013.

Willis, M. J., Melkonian, K., Pritchard, M., and Ramage, J.: Ice loss rates at the Northern Patagonian Icefield derived using a decade of satellite remote sensing, *Remote Sensing of Environment*, 117, 184–198, 2012a.

810 Willis, M. J., Melkonian, K., Pritchard, M., and Rivera, A.: Ice loss from the Southern Patagonian Ice Field, South America, between 2000 and 2012, *Geophysical Research Letters*, 39, L17 501, 2012b.